Proceedings of the Canadian Society for Mechanical Engineering International Congress
32nd Annual Conference of the Computational Fluid Dynamics Society of Canada
Canadian Society of Rheology Symposium
CSME/CFDSC/CSR 2025
May 25–28, 2025, Montréal, Québec, Canada

ID 495

Large-Eddy Simulation of Low- and High-Speed Turbulent Flows Using a High-Order CENO Finite-Volume Scheme

Thomas M. R. Dors* and Clinton P. T. Groth

Institute for Aerospace Studies, University of Toronto, 4925 Dufferin Street, Toronto, Ontario, Canada, M3H 5T6
*thomas.dors@mail.utoronto.ca

March 29, 2025

***Abstract*—**A density-based high-order Central Essentially Non-Oscillatory (CENO) finite-volume scheme in combination with minimally dissipative Riemann solver-based upwind numerical flux functions has been applied to both low- and high-speed canonical turbulent flow problems. In particular, implicit large-eddy simulation (LES) results were obtained by the numerical solution of the Favre-filtered form of the compressible Navier-Stokes equations for both the subsonic and supersonic Taylor-Green vortex (TGV) and decay of homogeneous isotropic turbulence (HIT) flows. The initial conditions for the latter were set to match those of previous low-speed wind tunnel experiments. DNS results for the HIT flow were also obtained through the implementation of a pseudo-spectral Fourier-Galerkin solver on a triply periodic cubic computational grid containing $2,048^3$ nodes which was used as a reference for the LES solutions. Published reference data was then used as a means of comparison for both of the TGV flow simulations considered in this study. For the subsonic TGV flow, the CENO scheme is shown to outperform a standard second-order finite-volume scheme by achieving a lower error in peak enstrophy at a reduced computational cost. Furthermore, the high-order CENO results obtained for the supersonic TGV flow show excellent agreement with the previous reference solutions. The high-speed TGV flow presents a unique challenge as it necessitates an accurate representation of small-scale turbulence while requiring sufficient numerical dissipation in the proximity of shocks. The CENO scheme addresses this challenge by employing a hybrid reconstruction procedure that transitions to a limited, low-order scheme for cells with under-resolved solution content. The latter are detected via a smoothness indicator, thereby ensuring that small turbulent flow scales in smooth regions are not excessively damped. Additionally, modified variants of the standard Roe flux are considered in this study and they are shown to provide significant reductions in numerical dissipation, as evidenced by the increased peak enstrophy for the TGV flow problem and a significantly improved prediction of the $-5/3$ slope in the spectral turbulence energy density compared with the results of the standard Roe flux in the case of the HIT decay problem.

***Keywords*—Large-Eddy Simulation (LES); High-Order Methods; Compressible Turbulent Flows; Computational Fluid Dynamics (CFD).**

I. Introduction

Accurate representation of the wide range of turbulent scales that high-fidelity simulations should produce remains a significant challenge. This is because the development of turbulent structures is extremely sensitive to errors originating from spatial discretization schemes. Specifically, for both large-eddy simulation (LES) and direct numerical simulation (DNS), standard-order methods underpredict flow scales in the higher-resolvable wavenumber range, which somewhat limits their applicability. This can be overcome by increasing the resolution of the computational grid; however, the cost of such an approach is significant. An alternative is to use high-order spatial discretization schemes, which provide improved accuracy, often at a cost less than their standard-order counterparts. In particular, high-order methods have low levels of numerical dissipation and dispersion, which enables accurate predictions of smaller turbulent length scales. This has motivated the continued use and development of high-order spatial discretization schemes for high-fidelity simulations of turbulent flows.

In this study, the high-order central essentially non-oscillatory (CENO) finite-volume scheme proposed by Ivan and Groth [1], [2] was combined with minimally dissipative Riemann solver-based numerical flux functions [3], [4] and used in the implicit LES of several canonical turbulent-flow problems. The CENO scheme has previously been successfully applied to incompressible low-Mach number viscous flows [5], LES of turbulent premixed combustion [6], steady subsonic laminar flows [1], [2], [7] and resistive MHD flows [8]–[10]. It is based on a hybrid solution reconstruction procedure that provides high-order accuracy in smooth regions and non-oscillatory transitions at discontinuities [1], [2]. This hybrid reconstruction procedure retains an unlimited high-order K-exact reconstruction for cells in which the solution is fully

resolved and reverts to the piecewise limited lower-order counterpart for cells with underresolved/discontinuous solution content [1], [2]. The transition in this hybrid reconstruction procedure is controlled by a smoothness indicator [1], [2].

II. Favre-Filtered Navier-Stokes Equations

LES simulations are considered herein based on the solution of the Favre-filtered form of the Navier-Stokes equations for a compressible gas. The latter can be achieved via the application of a low-pass spatial filtering procedure which yields the system of equations:

$$\frac{\partial \tilde{\rho}}{\partial t} + \frac{\partial \bar{\rho}\tilde{u}_j}{\partial x_j} = 0, \tag{1}$$

$$\frac{\bar{\rho}\tilde{u}_i}{\partial t} + \frac{\partial(\bar{\rho}\tilde{u}_i\tilde{u}_j)}{\partial x_j} - \frac{\partial \breve{\sigma}_{ij}}{\partial x_i} + \frac{\partial \bar{p}}{\partial x_j} = -\frac{\partial \tau_{ij}}{\partial x_j} + \frac{\partial}{\partial x_j}(\bar{\sigma}_{ij} - \breve{\sigma}_{ij}), \tag{2}$$

$$\begin{aligned} \frac{\partial(\bar{\rho}\tilde{E})}{\partial t} + \frac{\partial}{\partial x_j}\Big[(\bar{\rho}\tilde{E} + \bar{p})\tilde{u}_j + \tilde{q}_j - \breve{\sigma}_{ij}\tilde{u}_i\Big] \\ = -\frac{\partial}{\partial x_j}\Big(\gamma C_v Q_j + \tfrac{1}{2}\mathcal{J}_j - \mathcal{D}_j - (\bar{q}_j - \tilde{q}_j)\Big), \end{aligned} \tag{3}$$

where x_i and t are the position vector associated with physical space and time, $\tilde{\rho}$, $\tilde{u}_i$, $\tilde{E} = \bar{p}/(\gamma-1) + \widetilde{u_i u_j}/2$ are the Favre-filtered values of the gas density, flow velocity, total internal energy, and $\bar{p}$ is the filtered pressure. Here, $\breve{\sigma}_{ij}$ is the viscous stress tensor evaluated in terms of Favre-filtered quantities

$$\breve{\sigma}_{ij} = \mu(\tilde{T})\left(2\tilde{S}_{ij} - \frac{2}{3}\delta_{ij}\tilde{S}_{kk}\right), \tag{4}$$

and $\tau_{ij} = \bar{\rho}(\widetilde{u_i u_j} - \tilde{u}_i\tilde{u}_j)$ is the so-called subgrid-scale (SGS) stress tensor. The Favre-filtered heat flux is given by $\tilde{q}_j = -\tilde{\kappa}(\partial\tilde{T}/\partial x_j)$. The other remaining terms appearing the equations above are given by

$$Q_j = \bar{\rho}(\widetilde{u_j T} - \tilde{u}_i\tilde{u}_j), \tag{5}$$

$$\mathcal{J}_j = \frac{\bar{\rho}}{2}(\widetilde{u_j u_k u_k} - \tilde{u}_j\widetilde{u_k u_k}), \tag{6}$$

$$\mathcal{D}_j = \overline{\sigma_{ij}u_i} - \breve{\sigma}_{ij}\tilde{u}_i, \tag{7}$$

where Q_j is the SGS heat flux, $\mathcal{J}_j$ is the SGS turbulent diffusion, and $\mathcal{D}_j$ is the SGS viscous diffusion. The values of these SGS terms have been previously evaluated by Vreman *et al*. [11] and Martin *et al*. [12] where it was found that the influence of $(\bar{\sigma}_{ij} - \breve{\sigma}_{ij})$, $(\bar{q}_j - \tilde{q}_j)$, and $\mathcal{D}_j$ can all be considered negligible. The SGS heat flux and diffusion are then modeled to close the system of equations. First, using a gradient approximation, the SGS heat flux can be modeled as

$$\mathcal{Q}_j = \frac{\bar{\rho}\nu_t}{Pr_t}\frac{\partial\tilde{T}}{\partial x_j}, \tag{8}$$

and following the work of Knight *et al*. [13], the SGS diffusion can be defined as

$$\mathcal{J}_j = \tau_{jk}\tilde{u}_k. \tag{9}$$

Lastly, it is also possible to model the SGS stress tensor using a number of popular eddy-viscosity approaches, such as the standard and dynamic versions of the Smagorinsky model [14], [15]. However, in this study an implicit LES approach is adopted and no sub-grid modelling is used to explicitly model Q_j, $\mathcal{J}_i$ and τ_{ij}. The resulting system of equations therefore closely resembles the unfiltered form of the compressible Navier-Stokes equations. Both the filtering and subgrid modelling are achieved implicitly by the numerical method wherein errors from the spatial and temporal discretization schemes act as an additional equivalent SGS stress.

III. High-Order CENO Finite-Volume Method

The aforementioned Favre-filtered, compressible form of the Navier-Stokes equations can be written in the following form

$$\frac{\partial \mathbf{U}}{\partial t} + \vec{\nabla}\cdot\vec{\mathbf{F}} = \frac{\partial \mathbf{U}}{\partial t} + \nabla\cdot\left(\vec{\mathbf{F}}_{\mathrm{H}} - \vec{\mathbf{F}}_{\mathrm{E}}\right) = 0, \tag{10}$$

where $\mathbf{U}$ is the vector of conserved solution variables

$$\mathbf{U} = [\bar{\rho},\ \bar{\rho}\tilde{u},\ \bar{\rho}\tilde{v},\ \bar{\rho}\tilde{w},\ \bar{\rho}\tilde{E}]^{\mathrm{T}}, \tag{11}$$

and $\vec{\mathbf{F}}$ is the flux dyad which is the sum of the inviscid (hyperbolic) and viscous (elliptic) fluxes, $\vec{\mathbf{F}}_{\mathrm{H}}$ and $\vec{\mathbf{F}}_{\mathrm{E}}$ respectively. Following Ivan and Groth [1], [2], application of the high-order CENO finite-volume method to the integral form of Eq. (10) for hexahedral computational cells, ijk, of a multi-block body-fitted mesh results in the following semi-discrete form given by

$$\frac{d\overline{\mathbf{U}}_{ijk}}{dt} = -\frac{1}{V_{ijk}}\sum_{f=1}^{N_f}\sum_{m=1}^{N_{\mathrm{Gface}}}\Big(\omega(\vec{\mathbf{F}}_H - \vec{\mathbf{F}}_E)\cdot\vec{n}\Delta A\Big)_{i,j,k,f,m}, \tag{12}$$

where ΔA is the area of face f with $1 \le f \le N_f$ and ω is the face quadrature weighting coefficient for face f and quadrature point m. Equation (12) represents a coupled nonlinear system of first-order ordinary differential equations for the time evolution of the cell averaged values of conserved solution quantities, $\overline{\mathbf{U}}$, within each computational cell, ijk.

A. High-Order K-Exact Least-Squares Reconstruction

The CENO scheme uses the K-exact least-squares reconstruction of Barth [16] to achieve high-order spatial accuracy based on a K^{th}-order Taylor polynomial series expansion for a solution variable, U, about the centroid of each computational cell. As discussed by Ivan and Groth [1], [2], the order of the polynomial determines the spatial accuracy of the scheme. This K^{th}-order polynomial can be expressed as

$$U^K_{ijk}(\vec{x}) = \sum_{p_1=0}^{K}\sum_{p_2=0}^{K}\sum_{p_3=0}^{K}(\vec{x} - \vec{x}_{ijk})D_{p_1p_2p_3}, \tag{13}$$

where $\vec{x}$ is the cell centroid, U is the reconstructed solution variable, and K is the order of the polynomial. The spatial derivatives appearing in this expression, $D_{p_1p_2p_3}$, are the coefficients in the Taylor series expansion. Note that the error in the polynomial approximation is $\mathcal{O}(\Delta^{K+1})$. With sufficient quadrature points on each face, this implies that a K^{th} order polynomial achieves $K+1$ accuracy. This is true for the evaluation of the hyperbolic solution fluxes. However, the evaluation of solution gradients for the viscous fluxes

requires direct differentiation of the K^{th} order polynomial and, globally, this reduces the order of accuracy from order $K+1$ to order K. The target accuracy here is fourth-order and thus a $K=4$ reconstruction polynomial is used for a consistent fourth-order spatial discretization of the Navier-Stokes equations.

B. Inviscid/Hyperbolic Flux Evaluation

The inviscid or hyperbolic flux is evaluated at each cell interface by using a Riemann-solver based flux function in terms of the reconstructed solution variables based on the K-exact procedure within each computational cell as described above. Note also that the number of quadrature points per face must be increased from one (for second-order accuracy) to four (for fourth-order accuracy) to ensure the increased accuracy offered by the high-order reconstruction is retained in the numerical flux evaluation. Variants of the standard Roe flux [17], specifically LMRoe [3] and L^{2}Roe [4], are used here as they provide reduced levels of numerical dissipation in low-Mach regions of the turbulent flows.

C. Viscous/Elliptic Flux Evaluation

To maintain global $K^{\textbf{th}}$-order accuracy, solution gradients are computed by directly differentiating the K-exact polynomials [1], [2]. To achieve a unique value of the reconstructed solution and its gradient required for the evaluation of the viscous or elliptic fluxes at each face of a computational cell, simple arithmetic averages of the solution and its gradient are used given by

$$U_{i+\frac{1}{2},j,k} = \frac{(U_{left} + U_{right})}{2}\,, \tag{14}$$

$$\nabla U_{i+\frac{1}{2},j,k} = \frac{(\nabla U_{left} + \nabla U_{right})}{2}\,. \tag{15}$$

as proposed by Ivan and Groth [1], [2].

D. Smoothness Indicator

One of the defining properties of the CENO scheme is its ability to check for smooth solution content and thereby avoid the limiting of the solution gradients associated with smooth extrema. This is done through the use of a so-called smoothness indicator which extrapolates the K-exact polynomial reconstructed in cell, ijk, to a neighboring cell, pqr, and then compares this extrapolated polynomial with the original reconstructed polynomial in cell pqr. Formally, the smoothness indicator, α, is defined using

$$\alpha = 1 - \frac{\sum_{pqr}\left(U^K_{pqr}(\vec{x}_{pqr}) - U^K_{ijk}(x_{pqr},y_{pqr},z_{pqr})\right)^2}{\sum_{pqr}\left(U^K_{pqr}(x_{pqr},y_{pqr},z_{pqr}) - \overline{U}_{ijk}\right)^2}, \tag{16}$$

where $U^K_{ijk}(x_{pqr},y_{pqr},z_{pqr})$ is the reconstructed polynomial in cell, ijk, extrapolated to cell, pqr, and $U^K_{pqr}(x_{pqr},y_{pqr},z_{pqr})$ is the original reconstructed polynomial in cell pqr, and $\overline{U}_{ijk}$ is the average value of U for cell, ijk. For values of α approaching unity, the solution is deemed to be smooth and the high-order reconstruction is accepted; otherwise, the solution for cell ijk is deemed to be non-smooth and a standard piecewise limited linear reconstruction procedure is applied in the cell [1], [2]. Note that in the current study, the smoothness indicator is only used for the supersonic TGV as the subsonic flows are taken to be smooth.

IV. LES Results

Three canonical turbulent flows were investigated in this study. This includes the subsonic Taylor-Green vortex (TGV) [18], supersonic TGV [19] and decay of homogeneous isotropic turbulence (HIT) based on the experiment of Comte-Bellot and Corrsin (CB-C) [20]. Explicit Runge-Kutta time integration was used for all the results presented herein.

A. Subsonic Taylor-Green Vortex

The TGV flow problem provides a convenient validation problem for LES. Inviscid motions dominate the early stages followed by viscous diffusion which leads to a transition to turbulence. The initial conditions for the subsonic Taylor-Green vortex flow are given by [4]

$$\begin{aligned} u(\mathbf{x}, t=0) &= V_0\ \sin\!\left(\frac{x}{L}\right)\cos\!\left(\frac{y}{L}\right)\cos\!\left(\frac{z}{L}\right), \\ v(\mathbf{x}, t=0) &= -V_0\ \cos\!\left(\frac{x}{L}\right)\sin\!\left(\frac{y}{L}\right)\cos\!\left(\frac{z}{L}\right), \\ w(\mathbf{x}, t=0) &= 0\,, \end{aligned}$$

where V_0 is the reference velocity and L is a reference length scale defined such that $-\pi L \le x,y,z \le \pi L$ where the computational grid is a uniform periodic box with equal dimensions in each coordinate direction. The Reynolds number is defined as $Re = V_0 L/\nu$ and is set to 1,600. The Taylor-Green vortex test case can be extended to work with compressible flow solvers by defining an initial pressure field given by

$$p = p_0 + \frac{\rho_0 V_0^2}{16}\left[\cos\!\left(\frac{2x}{L}\right) + \cos\!\left(\frac{2y}{L}\right)\right]\left[\cos\!\left(\frac{2z}{L}\right) + 2\right],$$

where ρ_0 is the reference density. The fluid is assumed to be a perfect gas with specific heat ratio $\gamma = c_p/c_v = 1.4$ and Prandtl number $Pr = \mu c_p/\kappa = 0.71$. The reference Mach number is $M_0 = V_0/a_0 = 0.1$ with the speed of sound $a_0 = \sqrt{\gamma R T_0}$. The initial temperature field is uniform with $T = T_0$ and initial density field $\rho = p/RT_0$. The characteristic convective time, t_c, is defined as $t_c = L/V_0$, and the simulation is run for $t_{\text{final}} = 20t_c$. The reference pressure is $p_0 = \rho_0 R T_0$, where the reference density, ρ_0, is determined from the definition of the Reynolds number.

Several solution quantities of interest are analyzed when considering TGV flow simulations. This includes the volume averaged enstrophy, $\mathcal{E}$, which is defined as

$$\mathcal{E} = \frac{1}{\rho_0 V}\int_V \rho\frac{\boldsymbol{\omega}\cdot\boldsymbol{\omega}}{2}\mathrm{d}V\,, \tag{17}$$

where V is the volume of the computational domain and $\boldsymbol{\omega}$ is the vorticity vector. The global dissipation rate, ϵ, is based solely on the kinetic energy, E_k, and is given by

$$\epsilon = -\frac{dE_k}{dt}\,. \tag{18}$$

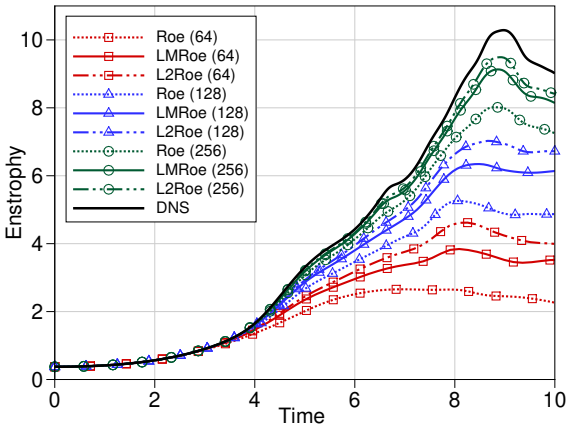

Figure. 1. Comparison of modified Roe flux functions for the time evolution of enstrophy for the subsonic TGV flow problem using the fourth-order CENO scheme on computational grids with 64^3 (red), 128^3 (blue) and 256^3 (green) cells.

TABLE. I
COMPUTATIONAL COSTS AND ERROR IN PEAK ENSTROPHY FOR THE SUBSONIC TAYLOR-GREEN VORTEX FLOW PROBLEM

Cells (N_i)	*Scheme*	*Order*	*Error (%)*	*CPU Time (hrs)*
64	CENO	4	58.7	377
128	LLR	2	63.9	415
128	CENO	4	32.5	3956
256	LLR	2	37.5	7974
256	CENO	4	7.97	33194
512	LLR	2	15.1	46493

The evolution of the kinetic energy, E_k, with time is also volume-averaged and is defined as

$$E_k = \frac{1}{\rho_0 V}\int_V \rho\frac{\mathbf{u}\cdot\mathbf{u}}{2}\mathrm{d}V\,, \tag{19}$$

where $\mathbf{u}$ is the velocity vector.

For the subsonic TGV flow problem, implicit LES results were obtained using both the proposed CENO scheme with fourth-order spatial accuracy and a second-order limited least-squares reconstruction scheme (LLR) on 64^3, 128^3 and 256^3 computational grids. The standard Roe flux, LMRoe and L^{2}Roe were also compared, the results of which can be seen in Fig. 1, where the time evolution of the enstrophy is shown. It is evident that L^{2}Roe flux function outperformed its counterparts.

The predicted temporal variation of the enstrophy comparing second-order LLR results to those of the fourth-order CENO scheme for the subsonic TGV problem is also given in Fig. 2. It is apparent that the high-order CENO scheme outperforms the LLR scheme on significantly coarser computational grids. For example, CENO results on a 128^3 grid show a higher level in peak enstrophy while costing nearly 40% less than LLR results obtained on a finer 256^3 grid. A summary of the computational costs for solving the subsonic TGV problem is presented in Table I. Figure 3 shows the time evolution of kinetic energy and dissipation rate; the differences between a coarse CENO and fine LLR result are not substantial. These results demonstrate that high-order solutions obtained on coarser grids can be both cheaper and more accurate than standard-order schemes on finer grids.

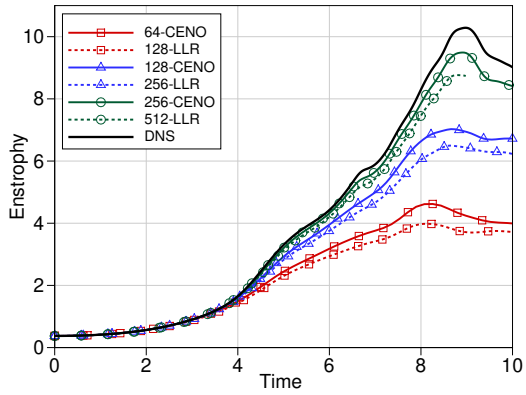

Figure. 2. Time evolution of enstrophy for the subsonic TGV flow problem using both second-order LLR and fourth-order CENO schemes with the L^{2}Roe numerical flux function on 64^3, 128^3, 256^3 and 512^3 computational grids.

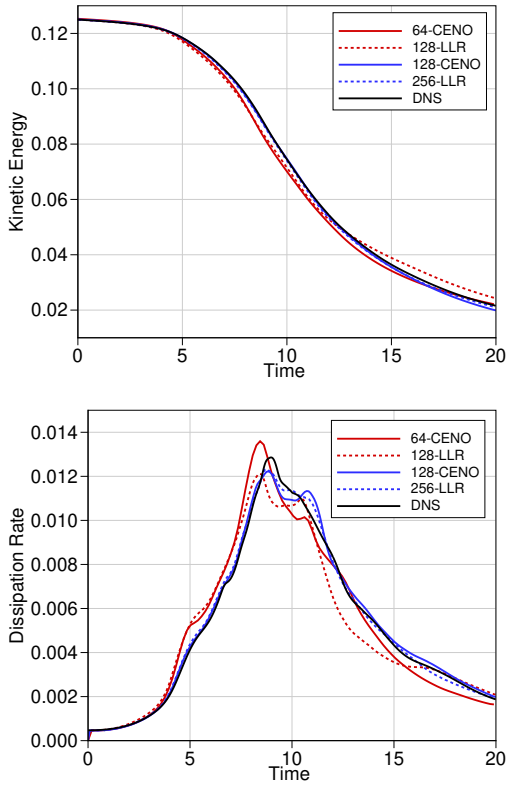

Figure. 3. Time evolution of kinetic energy (top) and energy-based dissipation rate (bottom) for the subsonic TGV flow problem using the second-order LLR and fourth-order CENO schemes on 64^3, 128^3 and 256^3 computational grids with the L^{2}Roe numerical flux function

B. Supersonic Taylor-Green Vortex

The TGV flow is further explored at a Mach number of 1.25 to assess the ability of the proposed CENO scheme in accurately representing both shocks and small scale turbulence. Following the work of Chapelier *et al.* [19], two additional diagnostics are used to analyze solutions to this flow problem. First, similar to enstrophy, solenoidal dissipation is used as a measure of the influence of the small scales and is defined as

$$\varepsilon_s = \frac{L^2}{ReU_0^2|V|}\int_V \frac{\mu(T)}{\mu_0}\boldsymbol{\omega}\cdot\boldsymbol{\omega}\,\mathrm{d}V\,, \tag{20}$$

TABLE. II
SUMMARY OF NUMERICAL METHODS COMPARED FOR THE SUPERSONIC TAYLOR-GREEN VORTEX FLOW PROBLEM

Solver	*Numerical Method*	*Order of Accuracy*	*Shock Capturing*
CENO	Central ENO	4	Local limiting
FLEXI	DGSEM	4	Subgrid FV
SD3DvisP	SD	4	LAD
SPADE	Central FD	8	Local upwinding
OpenSBLI	FD-TENO	6	TENO

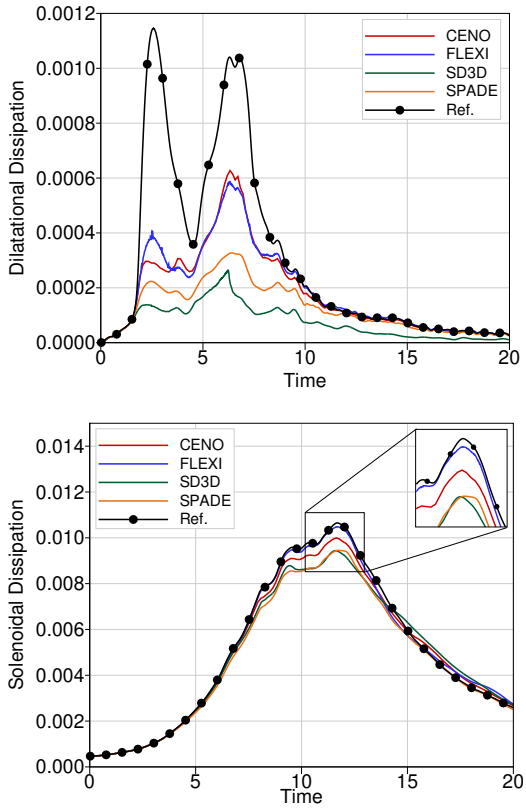

Figure. 4. Comparison of numerical methods for the time evolution of dilatational (top) and solenoidal (bottom) dissipation for the supersonic TGV flow.

where μ_0 is the reference dynamic viscosity at $t = 0$. The second is dilatational dissipation, which is a measure of the effects of compressibility, and is defined as

$$\epsilon_d = \frac{4L^2}{3ReU_0^2|V|}\int_V \frac{\mu(T)}{\mu_0}\left(\nabla\cdot\mathbf{u}\right)^2 \mathrm{d}V\,. \tag{21}$$

LES results obtained using a variety of schemes [19] are compared to those for the fourth-order CENO results in Fig. 4 and 5 for a 256^3 cubed computational mesh. Good agreement with the reference solutions is evident. The comparable numerical methods include results from discontinuous Galerkin (DG), finite-difference (FD), spectral difference (SD) and Targeted ENO (TENO) schemes (see Table II, LAD refers to localized artificial diffusivity). Note that the CENO scheme outperforms the other comparable numerical methods in that a sharp shock profile is obtained without any oscillations or smearing as depicted in Fig. 5.

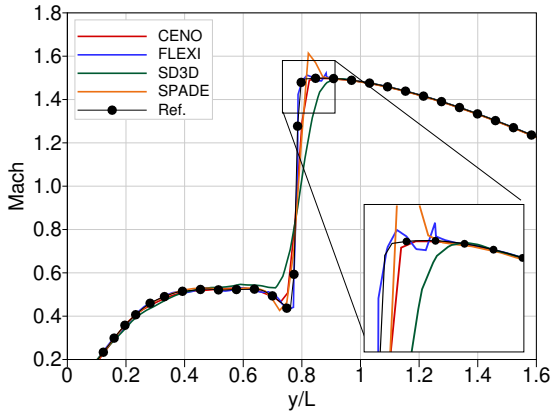

Figure. 5. Comparison of several numerical methods for the Mach number profiles on the line $x = z = 0$ at t_c = 2.5.

C. Comte-Bellot Corrsin Experiment

Finally, one of the more popular grid-generated wind tunnel turbulence experiments was done by Comte-Bellot and Corrsin (CB-C) [20] and has since been used as a benchmark for turbulence resolving numerical simulations. Measured energy spectra data was obtained at three downstream locations of a grid in a wind tunnel, thus providing a useful means for comparison with both LES and DNS results. Initial conditions for a LES or DNS solution, can be set to closely match the energy spectra measured at the first downstream location and comparisons can be made at both the second and third measurement points. A synthetic turbulent field is used in this research which is generated based on the method of Rogallo [21]. The simulations are run on a cubic grid with periodic boundary conditions on all six faces with uniform mesh spacing. Some researchers have proposed scaling the experimental data for a variety of reasons however, the approach of de Bruyn Kops and Riley [22] (which does not scale the data) is adopted as it has been shown that this method works quite well by optimizing the physical domain size to contain all the wavenumbers reported in the measured data of CB-C [20].

A comparison of the results obtained for the HIT problem using the various Roe flux functions is shown in Fig. 6 for both the energy spectra and decay of turbulent kinetic energy wherein the DNS solution was obtained with the implementation of a pseudo-spectral Fourier-Galerkin solver [23]. Additionally, Fig. 7 provides a comparison of fine LLR and coarse CENO results. Note that the CENO results obtained on the coarser 128^3 grid are nearly half the computational cost of the LLR scheme obtained using a 256^3 grid and show better agreement with the experimental data.

V. CONCLUSIONS

Both a standard second- and high-order finite-volume schemes in combination with low dissipative Roe-type flux functions have been applied to the solution of several canonical turbulent flows. For the subsonic TGV flow, the high-order CENO scheme has been shown to achieve higher levels of accuracy at a reduced cost compared to the second-order scheme and, for the supersonic case, ability of the CENO

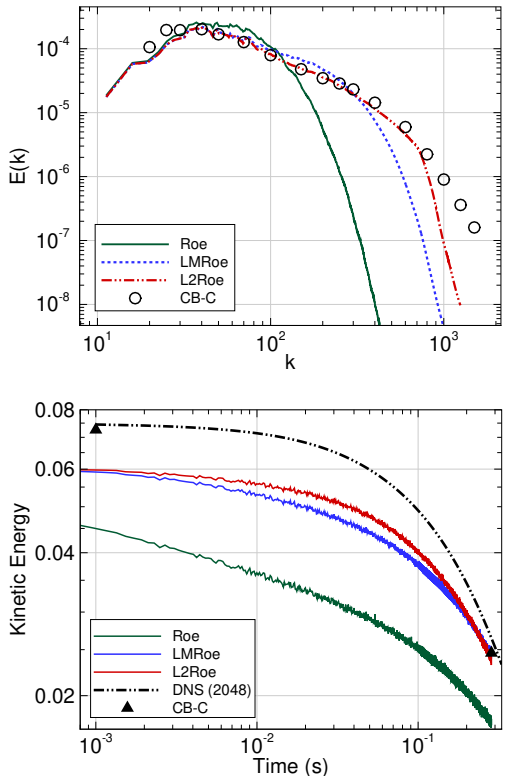

Figure. 6. Energy spectra at the second measurement location (top) and decay of turbulent kinetic energy (bottom) using the fourth-order CENO scheme with the modified Roe fluxes on a computational grid with 128^3 cells

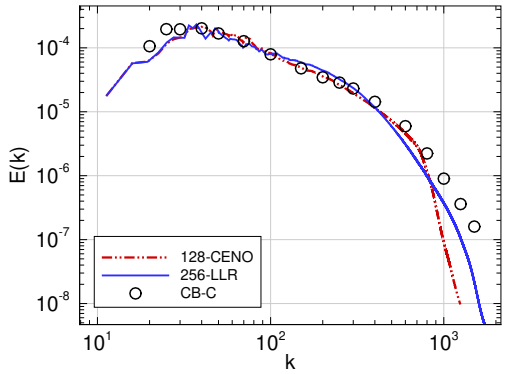

Figure. 7. Energy spectra at the second measurement location using the fourth-order CENO scheme and L^{2}Roe numerical flux function on a computational grid with 128^3 cells

scheme to capture shocks without excessive dissipation of the resolved turbulence has been demonstrated. Lastly, results for the CB-C experimental case have shown that the high-order CENO scheme on a coarser grid is more accurate than the standard second-order approach on a finer mesh while requiring less computational effort.

VI. Acknowledgements

Computational resources were provided by the SciNet High Performance Computing Consortium at the University of Toronto and the Digital Research Alliance of Canada through funding from the Canada Foundation for Innovation (CFI) and the Province of Ontario, Canada.

References

[1] L. Ivan and C. P. T. Groth. High-order solution-adaptive central essentially non-oscillatory (CENO) method for viscous flows. Paper 2011-0367, AIAA, January 2011.

[2] L. Ivan and C. P. T. Groth. High-order solution-adaptive central essentially non-oscillatory (CENO) method for viscous flows. *J. Comput. Phys.*, 257:830–862, 2014.

[3] F. Rieper. A low-Mach number fix for roe's approximate Riemann solver. *J. Comput. Phys.*, 230:5263–5287, 2011.

[4] K. Oßwald, A. Siegmund, P. Birken, V. Hannemann, and A. Meister. L2Roe: A low dissipation version of roe's approximate Riemann solver for low Mach numbers. *Int. J. Numer. Meth. Fluids*, 81(2):71–86, 2016.

[5] M. R. J. Charest and C. P. T. Groth. A high-order central ENO finite-volume scheme for three-dimensional turbulent reactive flows on unstructured mesh. Paper 2013-2567, AIAA, June 2013.

[6] L. Tobaldini Neto and C. P. T. Groth. A high-order finite-volume scheme for large-eddy simulation of turbulent premixed flames. Paper 2014-1024, AIAA, January 2014.

[7] L. Freret, C. N. Ngigi, T. B. Nguyen, H. De Sterck, and C. P. T. Groth. High-order ceno finite-volume scheme with anisotropic adaptive mesh refinement: Efficient inexact newton method for steady three-dimensional flows. *J. Comput. Phys.*, 94(48), 2023.

[8] A. Susanto, L. Ivan, H. De Sterck, and C. P. T. Groth. High-order central ENO finite-volume scheme for ideal MHD. *J. Comput. Phys.*, 250:141–164, 2013.

[9] L. Freret, L. Ivan, H. De Sterck, and C. P. T. Groth. High-order finite-volume method with block-based AMR for magnetohydrodynamics flows. *J. Sci. Comput.*, 79(1):176–208, 2019.

[10] T. B. Nguyen, H. De Sterck, L. Freret, and C. P. T. Groth. High-order implicit time-stepping with high-order CENO methods for unsteady three-dimensional CFD simulations. *Int. J. Numer. Meth. Fluids*, 94:121–151, 2022.

[11] B. Vreman, B. Geurts, and H. Kuerten. *A Priori* tests of large eddy simulation of the compressible plane mixing layer. *J. Engin. Math.*, 29(4):299–327, 1995.

[12] M. Pino Martín, U. Piomelli, and G. V. Candler. Subgrid-scale models for compressible large-eddy simulations. *Theoret. Comput. Fluid Dyn.*, 13:361–376, 2000.

[13] D. Knight, G. Zhou, N. Okong'o, and V. Shukla. Compressible large eddy simulation using unstructured grids. Paper 98-0535, AIAA, January 1998.

[14] J. Smagorinski. General circulation experiments with te primitive equations. I: The basic experiment. *Monthly Weather Review*, 91(3):99–165, 1963.

[15] M. Germano, U. Piomelli, P. Moin, and W. H. Cabot. A dynamic subgrid-scale eddy viscosity model. *Phys. Fluids*, 3:1760, 1991.

[16] T. J. Barth. Recent developments in high order k-exact reconstruction on unstructured meshes. Paper 93-0668, AIAA, January 1993.

[17] P. L. Roe. Approximate Riemann solvers, parameter vectors, and difference schemes. *J. Comput. Phys.*, 43:357–372, 1981.

[18] G. I. Taylor and A. E. Green. Mechanism of the production of small eddies from large ones. *Proc. Royal Soc. London A*, 158(895):499–521, 1937.

[19] J.-B. Chapelier, D. J. Lusher, W. Van Noordt, C. Wenzel, T. Gibis, P. Mossier, A. Beck, G.. Lodato, C. Brehm, M. Ruggeri, C. Scalo, and N. Sandham. Comparison of high-order numerical methodologies for the simulation of the supersonic Taylor-Green vortex flow. *Phys. Fluids*, 36(5):055146, 2024.

[20] G. Comte-Bellot and S. Corrsin. Simple Eulerian time correlation of full- and narrow-band velocity signals in grid-generated 'Isotropic' turbulence. *J. Fluid Mech.*, 48(2):273–337, 1971.

[21] R. S. Rogallo. Numerical experiments in homogeneous turbulence. Technical Memorandum 81315, NASA, September 1981.

[22] S. M. de Bruyn Kops and J. J. Riley. Direct numerical simulation of laboratory experiments in isotropic turbulence. *Phys. Fluids*, 10(9):2125–2127, 1998.

[23] W. M. van Rees, A. Leonard, D. I. Pullin, and P. Koumoutsakos. A comparison of vortex and pseudo-spectral methods for the simulation of periodic vortical flows at high Reynolds numbers. *J. Comput. Phys.*, 230:2794–2805, 2011.